Deep learning Using Physically-Informed Input Data for Wetland Identification

Gina L. O'Neil [a], Jonathan L. Goodall [a,b,*], Madhur Behl [b,a], Linnea Saby [a]

[a] Department of Engineering Systems and Environment, University of Virginia, Charlottesville, VA, 22904, USA
[b] Department of Computer Science, University of Virginia, Charlottesville, VA, 22904, USA

ABSTRACT

Automated and accurate wetland identification algorithms are increasingly important for wetland conservation and environmental planning. Deep learning for wetland identification is an emerging field that shows promise for advancing these efforts. Deep learning is unique to traditional machine learning techniques for its ability to consider the spatial context of object characteristics within a landscape scene. However, applying deep learning typically requires very large datasets for training the algorithms, which limits their application for many environmental applications including wetland identification. Using four study sites across Virginia with field delineated wetlands, we provide insight into the potential for deep learning for wetland detection from limited, but typical, wetland delineation training data. Our proposed workflow performs a wetland semantic segmentation using DeepNets, a deep learning architecture for remote sensing data, and an input dataset consisting of high-resolution topographic indices and the Normalized Difference Vegetation Index. Results show that models trained and evaluated for a single site were able to achieve high accuracy (up to 91% recall and 56% precision) and similar accuracy can be obtained for models trained across multiple sites (up to 91% recall and 57% precision). Through this analysis we found that, across all sites, input data configurations taking advantage of hydrologic properties derived from elevation data consistently outperformed models using the elevation data directly, showing the benefit of physically-informed inputs in deep learning training for wetland identification. By refining the wetland identification workflow presented in this paper and collecting additional training data across landscapes, there is potential for deep learning algorithms to support a range wetland conservation efforts.

1. Introduction

Wetlands are important ecosystems that are threatened by development, climate change, and pollution (Klemas, 2011). Wetland loss is both a global (Davidson, 2014) and national problem, as half of the wetlands of the conterminous U.S. have been lost since 1600 (Dahl et al., 1991). In the U.S., federal regulations, such as Section 404 of the Clean Water Act, play an important role in wetland protection. Laws require environmental impact assessments prior to land development and water resources projects, which entails the creation of detailed wetland surveys (Page and Wilcher, 1990). Conducting these surveys with the level of spatial resolution and accuracy needed to abide by federal regulations and meet the goal of avoiding adverse impact to wetlands can be time-consuming and costly. To support these efforts, methods for more rapidly identifying wetland locations are needed. Although manual surveys will continue to be the most accurate method to map wetlands, there is potential for supporting these efforts by using machine learning approaches, including deep learning, to identify wetland features at varying scales (Guo et al., 2017; Lang et al., 2013; Lang and McCarty, 2014).

Despite the many types of protected wetlands that exist, all wetlands can be identified by common features. These include the presence of hydrologic conditions that inundate the area, vegetation adapted for life in saturated soil conditions, and hydric soils (US Corps of Engineers, 1987). Researchers have demonstrated the ability to detect these features from multispectral imagery, radar, and Light Detection and Ranging (LiDAR) data (Guo et al., 2017). Multispectral imagery are the most commonly applied data in wetland studies (Guo et al., 2017; Klemas, 2011); however, spectral variables alone may be unable to distinguish wetlands due to spectral confusions from reflectance and backscattering (Dronova, 2015; Kim et al., 2011). LiDAR data are well-suited to complement multispectral analyses due to its wide, and growing, availability and demonstrated benefit to wetland mapping (Guo et al., 2017; Klemas, 2011; Kloiber et al., 2015; Lang and McCarty, 2014; Snyder and Lang, 2012). LiDAR returns can be interpolated to create high-resolution digital elevation models (DEMs), from which wetland indicators based on flow convergence and near-surface soil moisture can be derived (Lang et al., 2013; Lang and McCarty, 2014; Millard and Richardson, 2013, 2015; O'Neil et al., 2018, 2019). Moreover, researchers have shown the benefit of LiDAR DEM metrics as input

---

variables to traditional machine learning techniques, such as random forests, for wetland mapping and classification (e.g., Deng et al., 2017; Kloiber et al., 2015; Millard and Richardson, 2013; Millard and Richardson, 2015; O'Neil et al., 2018, 2019; Zhu and Pierskalla, 2016).

The successful coupling of LiDAR and multispectral imagery with traditional machine learning techniques for wetland identification is well-documented. However, deep learning for remote sensing studies, including wetland identification, is a new application space (Ma et al., 2017; Zhang et al., 2016) that shows promise for fulfilling the unmet need for wetland inventory creation. Deep learning architectures are modeled after the architecture of the mammal brain (Serre et al., 2007), where inputs are perceived and processed through multiple layers of abstraction. Convolutional neural networks (CNNs) (LeCun et al., 1998) are a representative form of deep learning that is used for visual recognition. CNNs utilize the spatial context of detected features to identify objects and classify scenes. The distinguishing element of CNN architectures are the convolutional layers, which convolve spatial filters over input images to identify patterns that are characteristic of target classes. Deep convolutional neural networks (DCNNs) (He et al., 2016; Krizhevsky et al., 2017; Simonyan and Zisserman, 2014) and fully convolutional neural networks (FCNs) (Long et al., 2015) are extensions of the CNN framework that can output dense pixel-wise classifications within images (i.e., semantic segmentation), where each pixel of the input image is assigned a class.

Since the formalization of the concept in 2006 (Hinton et al., 2006), deep learning has advanced the fields of speech recognition, medical diagnosis, and autonomous driving applications, and has since motivated new applications in environmental and water resources management (Liu et al., 2018; Pan et al., 2019; Shen, 2018; Zhang et al., 2016). Researchers have shown the ability of DCNNs, FCNs, and other CNN extensions to delineate urban and natural landscape classes using multispectral imagery and topographic data (Audebert et al., 2017, 2018), multispectral imagery and LiDAR point clouds (Xu et al., 2018), and multispectral imagery alone (Hu et al., 2018; Kemker et al., 2018b; Kemker et al., 2018a; Scott et al., 2017). Few researchers have applied DCNNs and FCNs specifically to wetland classification. These include Liu et al. (2018), who applied orthoimagery and elevation information to deep learning models for wetland segmentation. In addition, Rezaee et al. (2018) used multispectral imagery in a wetland deep learning model, and posited that predictions would improve with the incorporation of physical information from radar or LiDAR sources.

The typical need for massive validation sets to train deep learning models is a significant deterrent to environmental and water resources researchers (Shen, 2018; Zhang et al., 2016), as reliable training data is often lacking in these applications. This issue is especially prevalent for wetland identification that is intended to inform conservation and permitting efforts, where training data for computational models are ideally manually derived and confirmed by regulatory entities. The effects of training data limits for wetland semantic segmentation have been investigated by Liu et al. (2018), where comparisons were drawn for a single study area using DCNNs, FCNs, random forests, and support vector machines, with privately contracted aerial imagery and surface elevation information as input features. While this is an important stride in gaining insight into the training data needs for deep learning of wetlands, an analysis has yet to be done that utilizes freely-available data and is completed over multiple geographic regions.

The growing research area of deep learning for remote sensing applications shows promise for advancing wetland mapping. Although researchers have begun to show the potential for wetland identification at a high resolution using deep learning approaches, research gaps remain. Specifically, analyses are needed to identify the deep learning performance potential for different geographic regions when limited to relatively small quantities of verification data and freely available input data, which are typical in practice. We aim to contribute to this field by presenting a novel wetland identification methodology that implements a basic semantic segmentation architecture and is generalizable because

it leverages freely-available geospatial and remote sensing data. Our input data configuration consists of LiDAR DEM derivatives that describe geomorphologic and hydrologic contributors to wetland formation, as well as a commonly-used vegetative index. Using four study sites across Virginia, we build and evaluate several wetland models to demonstrate the potential for wetland semantic segmentation given typical training data resources. Through this research, we seek to answer the following questions.

i. Across geographically distinct study sites, what wetland prediction accuracy is achievable by building site-specific models from typically available amounts of wetland delineation training data?
ii. What is the potential for a single, combined-site model trained using data from across geographic regions to predict wetlands at each individual site?

2. Methodology

2.1. Study areas

Four study areas across Virginia, USA are used in this analysis (Fig. 1a). Data for each study area include the extents of wetland surveys and the surrounding Hydrologic Unit Code (HUC) 12 watershed (USGS, 2019) (Fig. 1b). The HUC 12 watersheds were used as processing extents and surveyed areas provided the validation data, also referred to as the study sites. The study areas span four level-III ecoregions. As shown in Table 1, the sites also vary by size, land cover, and topographic characteristics. Notable differences include the higher rate of development in sites 1 and 2, and the mild topography of Site 4. In addition, wetlands are much more abundant in Site 4, where the wetland to nonwetland ratio is 0.42, compared to less than 0.1 in the other sites. Note that all surveyed wetland types were merged into a single wetland category prior to use as verification data.

2.2. Input data

This study used publicly available LiDAR DEMs, National Agriculture Imagery Program (NAIP) aerial imagery, and field-mapped wetland surveys. LiDAR DEMs were obtained from the Virginia Information Technologies Agency (VITA) (VITA, 2016) as hydro-flattened, bare-earth DEMs. The LiDAR data used were collected and processed between 2010 and 2015 and have horizontal resolutions ranging from 0.76 m to 1.5 m. NAIP imagery are provided by the United Sates Department of Agriculture (Farm Service Agency, 2017). NAIP imagery were used to derive the NDVI. NAIP imagery contain four spectral bands (red, green, blue, and near-infrared) at a 1 m spatial resolution. Imagery used in this study were collected near the dates of wetland surveying, and images were resampled to match the resolution of the LiDAR DEMs, if necessary. Wetland delineations and survey limits were provided by the Virginia Department of Transportation (VDOT) in polygon vector format and served as validation data for this study. All verification wetlands were manually surveyed during summer months (May–August) between 2013 and 2016 by professional wetland scientists in compliance with transportation planning permitting. Wetland delineations for sites 2, 3, and 4 were also jurisdictionally confirmed by the US Army Corps of Engineers (USACE). Binary wetland/nonwetland geotiffs were created from these data, with resolutions matching those of the site LiDAR DEMs. Visual analyses of Google Earth images showed that the study site landscapes changed minimally between LiDAR acquisition and wetland delineation timeframes.

2.3. Wetland identification method

The wetland identification method consists of three main parts: preprocessing, feature creation, and semantic segmentation and accuracy assessment (Fig. 2). Input data required include high-resolution

DEM data, four-band aerial imagery, and validated wetland/nonwetland distribution data, all in geotiff format. From these data, topographic indices (curvature, Topographic Wetness Index, and Cartographic Depth-to-Water index) and the Normalized Difference Vegetation Index are calculated. These input features are merged into a single four-band composite grid. Smaller image tiles are created from the composite grid and validation data, and the pairs of corresponding image tiles are randomly separated into training and testing datasets. Finally, dense pixel-wise wetland predictions are made using a deep learning architecture created for remote sensing data, DeepNets for Earth Observation (Audebert et al., 2018), and the accuracy of wetland predictions is assessed. The main outputs are geotiff wetland predictions for each image tile and an accuracy report for the entire validation data area. The method was implemented using open source Python libraries and is available under an MIT license (see Software Availability section).

2.4. Preprocessing

DEM preprocessing was necessary to create an improved land surface representation from which to calculate indicators of wetland geomorphology. First, DEM smoothing is performed, which is necessary to addresses microtopographic noise. Microtopographic noise is common in high-resolution DEMs and can be representative of either erroneous data or true variations in the elevation of vegetated surfaces (Jyotsna and Haff, 1997). DEM conditioning is then executed, which is necessary prior to modeling hydrologic flow paths, as it addresses topographic depressions (Jenson and Domingue, 1988; O'Callaghan and Mark, 1984). Topographic depressions interfere with overland flow path modeling by creating discontinuities in flow paths and accumulating water, which negatively influences modeled watershed processes (Grimaldi et al., 2007; Lindsay, 2016; Lindsay and Creed, 2005). DEM conditioning is particularly important for hydrologic modeling from
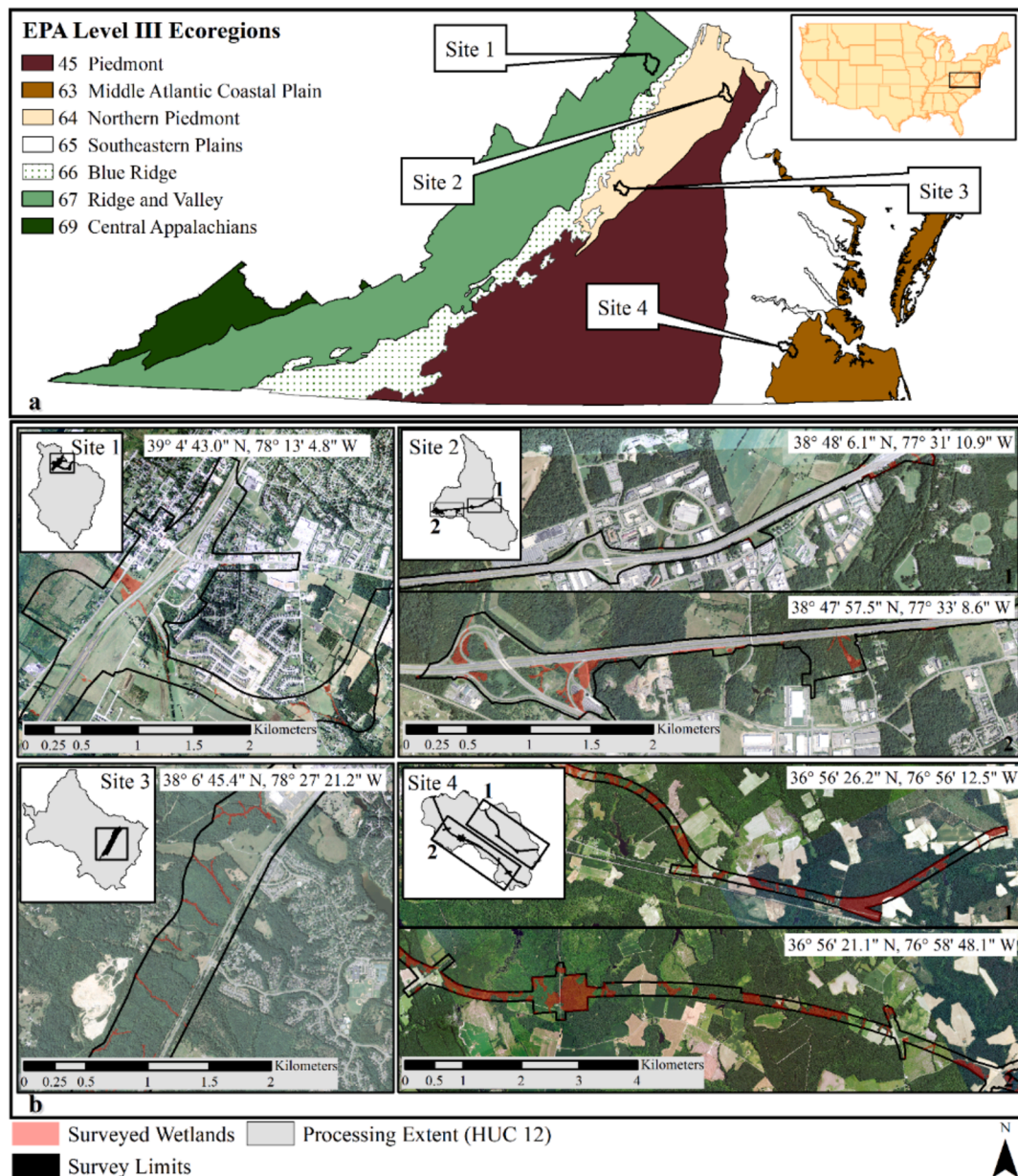

Fig. 1. Four study areas spanning four level III ecoregions in Virginia, USA (a). Each study area includes the wetland survey limits, referred to as study sites, and the encompassing HUC 12 watershed, used as the processing extent (b). Reprinted from "Effects of LiDAR DEM Smoothing and Conditioning Techniques on a Topography-Based Wetland Identification Model" by O'Neil et al. (2019), Water Resources Research, 55 (5), 4343–4363. Ecoregion data source: US EPA Office of Environmental Information. Aerial imagery data source: NAIP Digital Ortho Photo Image.

Table 1

Characteristics of each study site, including dominate land cover, topographic characteristics, and surveyed wetland distributions. Reprinted from "Effects of LiDAR DEM Smoothing and Conditioning Techniques on a Topography-Based Wetland Identification Model" by O'Neil et al. (2019), Water Resources Research, 55 (5), 4343–4363.

	Site 1	Site 2	Site 3	Site 4
Dominating Land Cover[a]	Turf Grass (35%), Developed (22%), Cultivated (20%), Forested (19%)	Developed (36%), Turf Grass (31%), Forested (21%)	Forested (73%), Developed (9%), Cultivated (9%)	Forested (66%), Cultivated (18%), NWI Wetland (9%)
Verification Area (km²)	2.8	1.6	1.8	5.6
Min. Elevation[b] (m)	209	46	101	10
Max. Elevation (m)	241	107	178	42
10th Percentile Slope[c] (m/m)	0.02	0.01	0.04	0.01
90th Percentile Slope[c] (m/m)	0.14	0.20	0.26	0.06
Mean Slope[c] (m/m)	0.07	0.08	0.14	0.03
Wetland: Nonwetland (m²/m²)	0.03	0.06	0.02	0.42
Dominating Cowardin Wetland Type(s)[d]	Palustrine Emergent (50%), Streams (20%)[e]	Palustrine Forested (44%), Palustrine Emergent (33%)	Palustrine Forested (56%), Streams (43%)	Palustrine Forested (88%), Palustrine Shrub (9%)

[a] Source: Virginia Information Technologies Agency (VITA) Land Cover classifications (https://www.vita.virginia.gov/integrated-services/vgin-geospatial-services/land-cover/).

[b] In sites 1, 2, and 4, verification area varied slightly due to edge effects of applying filtering to DEMs.

[c] Slope information was calculated from LiDAR DEMs resampled to a 5 m resolution to reduce effect of raw DEM noise on slope information.

[d] Values are approximate and according to VDOT wetland surveying reports.

[e] Wetland type for remaining 30% of wetland area was not reported.

high-resolution DEMs, as researchers have found that sensitivity of hydrologic parameter extraction to conditioning technique increases significantly with DEM resolution (Woodrow et al., 2016). Although many techniques have been proposed for both DEM smoothing and conditioning, we apply the Perona-Malik smoothing and A* least-cost path conditioning. This preprocessing combination was found to considerably improve wetland identification for the study sites in a prior study (see O'Neil et al., 2019). The Perona-Malik filter (Perona and Malik, 1990) performs a nonlinear, anisotropic diffusion that preserves feature edges by penalizing smoothing across estimated feature boundaries (Passalacqua et al., 2010a; 2010b). Perona-Malik smoothing was implemented using code from the nonlinear filtering module from PyGeoNet, an open source software for automatic channel network extraction from DEMs (Passalacqua et al., 2010a; Sangireddy et al., 2016). The A* least-cost path algorithm (Hart et al., 1968) determines the least-cost drainage paths through unaltered terrain and out of sinks, thus avoiding unnecessary modification of the input DEM (Metz et al., 2011). The A* conditioning method was executed using the GRASS GIS *r.watershed* module (GRASS Development Team, 2017; Metz et al., 2011).
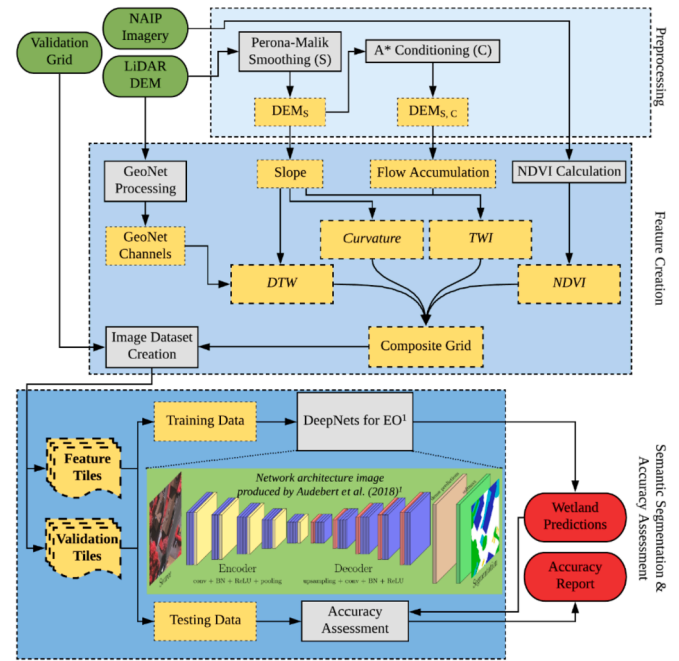

Fig. 2. Overview of the proposed wetland identification method. Green shapes indicate input data, grey shapes indicate processes, yellow shapes indicate intermediate output, and red shapes indicate final model output.
[1] Audebert, N., Le Saux, B., & Lefèvre, S. (2018). Beyond RGB: Very high resolution urban remote sensing with multimodal deep networks. ISPRS Journal of Photogrammetry and Remote Sensing, 140, 20–32.

2.4.1. Feature creation

2.4.1.1. Topographic features. In a prior study, we concluded that the curvature, Topographic Wetness Index (TWI) and Cartographic Depth-to-Water index (DTW) are successful topographic metrics for wetland identification for our study sites (O'Neil et al., 2018, 2019).

Curvature of a surface can describe the degree of convergence and acceleration of flow (Moore et al., 1991), and studies have shown its capability to indicate saturated and channelized areas (Ågren et al., 2014; Hogg and Todd, 2007; Kloiber et al., 2015; Millard and Richardson, 2015; O'Neil et al., 2018, 2019; Sangireddy et al., 2016). Here we use laplacian curvature, defined as the second derivative of the elevation grid. Laplacian curvature has been shown to favor the extraction of natural channels rather than artificial drainage paths, and to more effectively identify channels in flat, developed landscapes compared to alternative curvature forms (Passalacqua et al., 2012). Thus, we found the laplacian curvature to be most suitable for our study areas which all encompass corridor projects and are partially developed (O'Neil et al., 2019). The curvature grid is created from the smoothed DEM using code adopted from PyGeoNet (Passalacqua et al., 2010a; "PyGeoNet," 2019; Sangireddy et al., 2016).

The ability of the TWI to indicate saturated areas is well-documented in the literature (Ågren et al., 2014; Lang et al., 2013; Millard and Richardson, 2015; Murphy et al., 2009; O'Neil et al., 2018, 2019). The TWI relates the potential for an area to accumulate water to its tendency to drain water, defined as

$$TWI = \ln\left(\frac{\alpha}{\tan \beta}\right) \tag{1}$$

where α is the specific catchment area (contributing area per unit contour length) and $\tan(\beta)$ is the local slope (Beven and Kirkby, 1979). The TWI was created from the smoothed, conditioned DEM using the *r.watershed* program of GRASS GIS. This module calculates the α term using the multiple flow direction algorithm (Holmgren, 1994) and the β

term using a GRASS GIS-calculated slope.

Researchers have demonstrated the capability of the DTW to capture saturated areas as well (Murphy et al., 2007, 2009; 2011; O'Neil et al., 2018, 2019; Oltean et al., 2016; White et al., 2012). The DTW assumes that the likelihood for soil to be saturated increases with its proximity to surface water, in terms of distance and elevation (Murphy et al., 2007). Calculated on a per-pixel basis, the DTW is defined as

$$DTW\ (m) = \left(\sum \left(\frac{dz_i}{dx_i} \right) a \right) {}^*x_p \qquad (2)$$

where $\frac{dz}{dx}$ is the downward slope of pixel i along the least-cost (i.e., slope) path to the nearest surface water pixel, a is a factor accounting for flow moving parallel or diagonal across pixel boundaries, and x_p is the pixel resolution (Murphy et al., 2007). Inputs required to calculate the DTW include a slope grid, representing cost, and a surface water grid, representing the source from which distance is calculated. We create the surface water grid directly from the LiDAR DEM using PyGeoNet, which performs a statistical analysis of curvature and uses geodesic minimization principles to predict stream lines (Passalacqua et al., 2010a; Sangireddy et al., 2016). Visual analyses showed that streams created by PyGeoNet better aligned with aerial imagery, compared to national hydrography data (i.e., NHD streams) and streams generated from the flow initiation threshold method (Band, 1986; O'Callaghan and Mark, 1984; Tarboton, 1991) that is commonly used. PyGeoNet was executed using parameters suggested for engineered landscapes (see Sangireddy et al., 2016), which was found to produce accurate results across all sites in prior wetland model development (O'Neil et al., 2019). The PyGeoNet streams and slope grid were used as inputs to the GRASS GIS r.cost module (GRASS Development Team, 2017) to create the DTW grid.

2.4.1.2. NDVI. The NDVI is a commonly-used spectral index that relates plant biomass and stress and separates wet versus dry areas (Klemas, 2011; Ozesmi and Bauer, 2002). Researchers have used the NDVI as a wetland indicator in traditional machine learning frameworks (Corcoran et al., 2013; Dronova, 2015; Dronova et al., 2011; Guo et al., 2017; Mui et al., 2015; Rampi et al., 2014; Tian et al., 2016), as well as for general land cover classifications using deep learning frameworks (Audebert et al., 2017, 2018; Lee et al., 2019; Xu et al., 2018). The NDVI utilizes the red and the near-infrared bands (Carlson and Riziley, 1997), defined as

$$NDVI = \frac{Infrared - Red}{Infrared + Red} \qquad (3)$$

The red band indicates surface layer chlorophyll, and therefore surface conditions of plants, and the near-infrared band is reflected from the inner leaf cell structure, indicating the abundance of plant tissue (Klemas, 2011). To calculate the NDVI, Eq. (3) was executed using NumPy operations and the appropriate NAIP imagery bands.

2.4.1.3. Image dataset creation. The image dataset creation produces two sets of image tiles: i) feature tiles representative of the composite grid of input features, and ii) validation tiles representative of ground truth wetland and nonwetland locations. Due to the irregular shapes of the field surveys, NoData pixels existed within the rectangular extent of the validation data. Rather than reduce our validation data to an extent without unverified area, NoData pixels were treated as an additional target landscape class. Thus, all pixels in the validation data were categorized as NoData (0), nonwetland (1), or wetland (2) as a first step in the image dataset creation process.

To build the dataset of feature tiles, each band of the composite grid is rescaled to a range of 0–1, per the requirements of the DeepNets algorithm. Rescaling the NDVI band was nontrivial, as these values have global minimum and maximum of −1 and 1. Conversely, the range of values for each of the topographic features depends on the landscape they are calculated from, therefore it was necessary to assume global

Table 2
Minimum and maximum values used to scale each input feature to a range of 0–1. Minimum and maximum values were assumed for the TWI, curvature, and DTW from statistical analyses.

	TWI	Curvature	DTW	NDVI
Global Minimum	0	−3	0	−1
Global Maximum	30	3	35	1

minimum and maximum values. The range of each topographic input was analyzed across the study sites, and global minimum and maximum values that encompassed roughly 90% of the values were chosen. Note that only global maximum values had to be assumed for the TWI and DTW, which both have global lower bounds of 0 or nearly 0. Although this step generalizes portions of the study areas, this occurs only where there are extreme topographic features that occur infrequently. In addition, by limiting the range applied to each topographic input feature rather than choosing extreme, but encompassing, values, the significance of the relative distance between values is minimally affected. The minimum and maximum values used to rescale topographic features and the NDVI to a range of 0–1 are shown in Table 2.

Following these steps, the categorized validation grid and scaled composite grid were each separated into image tiles of size 320 x 320 pixels. We chose the 320-pixel size constraint to balance the desire to use image tiles large enough to depict heterogeneous landscapes and the need to separate the study site into enough images to sample training and testing tiles that were randomly dispersed. Feature and labeled image tiles sets were not considered for either training or testing if more than 80% of the area was populated with NoData pixels.

2.4.2. Semantic segmentation model: DeepNets for Earth Observation

Our model performs a semantic segmentation of input images, where each pixel of an input image is labeled as either NoData, nonwetland, or wetland. That is, a trained semantic segmentation model will assign a class prediction to each pixel in an image, however different instances of target class objects are not defined (i.e., instance segmentation).

As an initial step in developing a deep learning wetland model, the current work is intended to demonstrate the suitability of a CNN to identify planning-scale wetlands in the landscape. We implemented a multimodal deep network, DeepNets for Earth Observation, for semantic segmentation classification (Audebert et al., 2017). DeepNets has emerged as a state-of-the-art tool for segmentation of high-resolution remote sensing data (Demir et al., 2018), and has been implemented and validated for automating segmentation of remote sensing data (Audebert et al., 2016, 2017, 2018).

Although DeepNets was chosen as a vehicle to address the guiding research questions of this work, it is among several deep learning architecture currently achieving competitively in semantic segmentation of satellite imagery. Ghosh et al. (2018) applied a Stacked U-Nets architecture to achieve high-quality satellite imagery segmentation with relatively few prediction parameters. Volpi and Tuia (2016) use a CNN to segment very high-resolution imagery to achieve F1 scores of about 85%. Marmanis et al. (2018) propose a downsample-upsample and achieve similar results. While each of these approaches are likely to achieve good results with wetlands segmentation, DeepNets achieved slightly higher results on segmentation of benchmark imagery datasets (Demir et al., 2018), thus it was adopted for this study. An important future step in progressing this research would be to perform a comparative analysis of other emerging deep learning techniques for wetland segmentation.

As a starting point in the development of our deep learning wetland model, the baseline DeepNets architecture is implemented here (Audebert et al., 2018, 2019). DeepNets builds on the SegNet architecture (Badrinarayanan et al., 2017) and is implemented using PyTorch (Paszke et al., 2017). SegNet produces predictions with the same resolution as the input image by using an encoder-decoder structure, making

it well-suited for classification of landscape objects from georeferenced images (Audebert et al., 2018; Badrinarayanan et al., 2017). The encoder portion of SegNet is based on the convolutional layers of VGG-16 (Simonyan and Zisserman, 2014), and consists of convolutional layers, batch normalization, a rectified linear unit, and max-pooling. As shown in the inset image (defined by Audebert et al., 2018) in Fig. 2, the decoder is structurally symmetrical to the encoder. Pooling layers are replaced with unpooling layers that relocate pixel activations from the smaller feature maps to corresponding indices of zero-padded upsampled images. Convolution blocks are then used to densify the sparse pixel activations. This sequence of unpooling and convolutions is repeated until feature maps reach the original spatial resolution. Following this, a softmax layer is used to compute multinomial logistic loss. Another feature of the DeepNets approach is the generation of predictions at several resolutions, and the calculation of loss at these intermediate resolutions. In doing so, the DeepNets model predicts a semantic map at full resolution as well as smaller resolutions, which are averaged together to obtain a final full-resolution semantic prediction. Lastly, a sliding window approach is used to extract smaller patches within each input image, which acts as data augmentation. For further details on the DeepNets architecture, we direct readers to Audebert et al. (2018).

Following procedures demonstrated by Audebert et al. (2016, 2017, 2018), we incorporate the NDVI and elevation data into our DeepNets model. However, rather than using the original elevation grid as an input, we guide the learning of the model by deriving specific geomorphic and hydrologic features from the DEM as inputs. This strategy was chosen following a hypothesis that wetland predictions would improve if a deep learning model trained from explanatory variables that are specific to wetlands. In our implementation of DeepNets, we also applied class weights, which are related to the importance of correct predictions for a specific class when calculating the loss. We used this feature to account for the imbalance between the wetland and nonwetland classes across all sites, as well as to decrease the importance of NoData areas. Lastly, we allow for data augmentation in the form of mirroring images and flipping the orientation. Parameters for the DeepNets model incorporated into our wetland model workflow are given in Table 3. Note that these parameters were chosen as starting points to be later refined through additional model testing.

2.4.3. Accuracy assessment

In line with the intended environmental planning and permitting application, accuracy metrics were selected considering the higher importance of true positive (i.e., wetland) predictions versus true negative (i.e., nonwetland) predictions to wetland conservation. Model performance was evaluated in terms of wetland recall and wetland precision, calculated using the Scikit-learn Python library (Scikit-learn Developers, 2017).

Recall, also known as the true positive rate, represents the percentage of true wetlands that were predicted, and is defined as

$$Recall = \frac{True\ wetland\ predictions}{Total\ true\ wetlands}. \tag{4}$$

Recall can be considered the priority indicator of model performance given the importance of the minority wetland class, a choice also supported by statistical literature (Branco et al., 2016; Chen et al., 2004;

Sun et al., 2007). Precision is used to account for model overprediction. Unlike the commonly-used specificity, precision is not biased by large numbers of true negative instances, and therefore can be considered more representative for imbalanced scenarios (Branco et al., 2016; Sun et al., 2007). Precision represents the percentage of wetland predictions made that were correct, defined as

$$Precision = \frac{True\ wetland\ predictions}{Total\ wetland\ predictions}. \tag{5}$$

It should be noted that the appropriate selection of accuracy metrics remains an open problem not only for semantic segmentation, but for classification tasks in general, and additional criteria have been proposed and widely used. We found recall and precision to be more suitable for model assessment compared to commonly used options, such as overall accuracy, Kappa statistic, and Matthews Correlation Coefficient (MCC). When using overall accuracy, detection rate of the minority class has a lower impact than that of the majority class (Branco et al., 2016; Chen et al., 2004), misrepresenting a wetland model predicting all nonwetland instances as very accurate. Moreover, the Kappa statistic is biased by sample size, and can increase as the wetlands to nonwetlands ratio increases, even if wetland recall decreases (Ali et al., 2014; Byrt et al., 1993). Both overall accuracy and the Kappa statistics have been omitted from wetland classification studies for these reasons (Baig et al., 2014; Zhu and Pierskalla, 2016). Although the MCC metric has been shown to be suitable for imbalanced scenarios (e.g., Boughorbel et al., 2017), its takes into account the number of true negative samples.

2.5. Experimental setup

2.5.1. Addressing research question 1: creating site-specific models

Experiments 1 and 2 (Fig. 3A) were designed to offer insight into potential wetland accuracy given varying sizes of reliable training sets, evaluated over four geographic regions. In Experiment 1, we created models that sample training images from the area to be mapped (i.e., site-specific models). For each site, 70% of eligible image sets were randomly selected, producing the maximum training set size available, which varied based on site size (Table 4). To compare how models of different ecoregions perform given the same training resources, site-specific models were created and evaluated at each threshold of training set size. Experiment 2 applied the site-specific models created through Experiment 1 (those using the maximum training set size) to predict wetlands in the other sites. Thus, Experiment 2 represents the scenario where a pretrained wetland model is applied for a new area for which training data is unavailable.

2.5.2. Addressing research question 2: creating combined-site models

Experiments 3 and 4 (Fig. 3B) aim to evaluate the potential for improving wetland accuracy by incorporating training data from different geographic regions into a single model. In Experiment 3, a wetland model is trained using the largest training sets available from each site (i.e., "general model"). In Experiment 4, a model is created using the maximum training data from two sites within the same ecoregion: Site 2 and Site 3 (i.e., "ecoregion model"). Both experiments aim to gain insight into the change in wetland predictions when the model learns wetland characteristics that exist for a range of landscapes.

3. Results

3.1. Performance of site-specific models

For Experiment 1, site-specific models were built using training data quantities ranging from 9 to 77 images, depending on validation data extents (Fig. 4). The resulting 10 sets of wetland predictions were evaluated for the testing area complementing the training data quantity used. Results show that the best performing models for each site were those trained using the maximum training set size available, equal to

Table 3
Parameters for the DeepNets implementation used in all performed experiments.

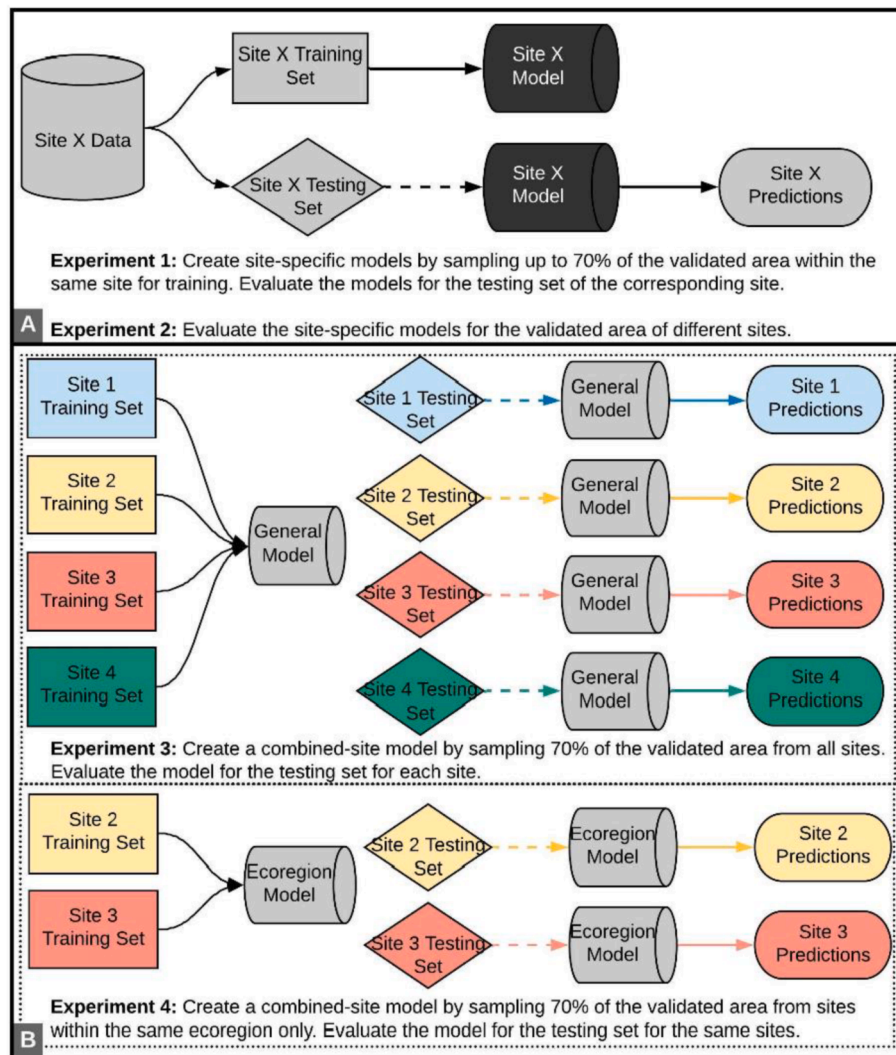|	
Image tile size (# pixels)	320, 320
Sliding window size (# pixels)	64, 64
Sliding window stride (# pixels)	8
Base learning rate	0.01
Momentum	0.9
Weight decay	0.005
Training epochs	100
Class weights [NoData, Nonwetland, Wetland]	[0.02, 0.08, 0.9]

Fig. 3. Methodology followed for the four experiments designed to address the study research questions.

Table 4
Maximum number of training images available per site when randomly sampling 70% of the eligible validated area. Each labeled image used for training has a resolution of 320 x 320 pixels.

Site	Maximum training sets size (# images)
Site 1	31
Site 2	9
Site 3	28
Site 4	77

Fig. 4. Wetland mapping accuracy resulting from Experiment 1, where site-specific models were created using several training data sizes depending on site availability.

70% of the validation area. Conversely, the lowest performing models across all sites occurred when using the fewest training data, nine images. The Site 4 model trained with 77 images achieved the highest wetland recall and precision across all site models. The Site 4 model also outperformed other sites when limited to the same number of training images (Fig. 4). The overall lowest performing model was built for Site 2, which also had the smallest training dataset available, only nine images.

While the improvements in prediction accuracy as training data increased were expected, intermediate changes in accuracy were inconsistent. For Site 3, recall increased considerably (46%–85%) and precision increased slightly (17%–20%) when increasing training images from 9 to 28. However, changes in model accuracy were less significant for Site 1, where the most notable accuracy improvement occurred when increasing training data from 28 to 31 images, which
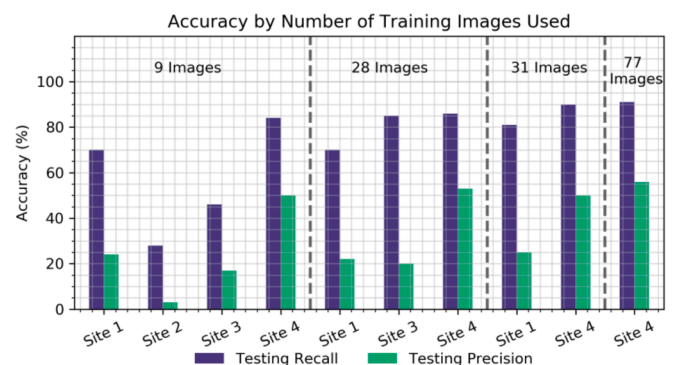
increased recall from 70% to 81% and precision from 22% to 25%. Models built for Site 4 performed consistently, maintaining high performance regardless of training set sizes ranging from 9 to 77 images. For Site 4, recall only varied between 84% and 91% and precision between 50% and 56%. It was unexpected that Site 4 did not improve more notably when increasing the training dataset from 31 to 77 images, as

this was the largest increase in training set studied. This may be due to the fact Site 4 has the most balanced wetland to non-wetland areas, so fewer training images are needed to create an accurate model.

3.2. Using site-specific models to predict wetlands in other sites

Experiment 2 resulted in an additional 12 sets of results, where the best performing site-specific models (i.e., those trained with the maximum training data set size) were used to predict wetlands in the other sites. The evaluation of these trials represents wetland prediction accuracy for the entirety of the site validation area, and the results achieved by applying the site-specific models for their own areas are also shown for reference (Fig. 5). In most cases, utilizing training information from a different area, even if this represented a greater quantity of data, did not improve predictions compared to those resulting from a model trained for its own area. Site 2 was the exception for this trend, as both recall and precision improved when using any of the models built for other sites, compared to using the Site 2 model. Moreover, the Site 2 model produced more accurate wetland predictions when applied to the other sites, compared to its own testing area. Although the predictions for others sites resulting from the Site 2 model were still among the lowest accuracies per site, this suggests there may be topographic or spectral confusion between Site 2 training and testing data. Also, there was an unexpected increase in precision when applying the Site 1 model versus the Site 4 model for Site 4 predictions. However, since both wetland precision and wetland recall should be considered when summarizing model performance, the significantly greater recall achieved by the Site 4 model leads us to conclude that the Site 4 model outperformed the Site 1 model here. Lastly, the Site 4 model resulted in the highest recall scores and among the lowest precision scores across all trials for sites 1, 2, and 3. This reflects a tendency of the Site 4 model to overpredict wetlands in other sites. This may be because Site 4 includes large, areal wetlands common in the coastal plain given its low relief topography, but uncommon in the other three sites that are outside of the coastal plain.

3.3. Performance of combined-site models

Experiment 3 resulted in the general model, trained with the maximum available training images from each site. When applying the general model to Site 1 testing areas, recall increased from to 81%–89% and precision decreased from 25% to 18%, relative to the best

performing Site 1 model (Fig. 6). For Site 2 testing areas, the general model considerably improved wetland recall (28%–40%) and minimally changed precision (3%–2%), compared to the best performing site-specific model (Fig. 6). The general model produced worse predictions than the site-specific model for Site 3, decreasing recall from 85% to 73% and precision from 20% to 15%. The general model performed nearly the same for Site 4 compared to the site-specific model, where recall remained high at 91% and precision increased by a small margin from 56% to 57%. These results suggest that a general model trained with data collected across all sites would not be a suitable method for wetland prediction, at least with the current methodology and data availability.

Experiment 4 resulted in the ecoregion model, trained with the maximum available training images from sites 2 and 3, which share the Northern Piedmont ecoregion. This experiment tested the idea that a general wetland classification may be possible, but only within a single ecoregion and not across ecoregions as was attempted in Experiment 3. For Site 2, the ecoregion model produced worse predictions than the general model and the site-specific model, with recall decreasing to 21% and precision remaining nearly the same at 2% (Fig. 6). In contrast, the ecoregion model improved wetland recall and precision for Site 3 (77%
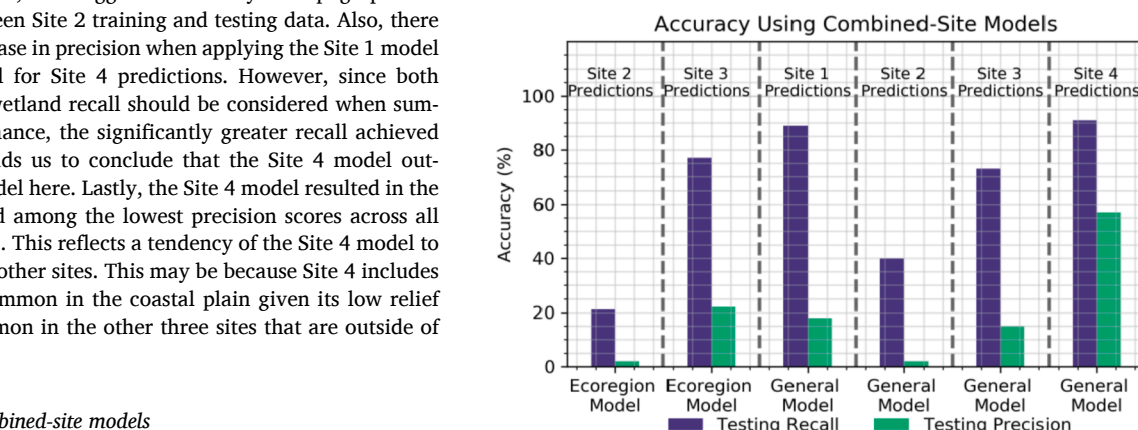

Fig. 6. Wetland mapping accuracy resulting from Experiment 3, which used training data from all sites to create a general model, and Experiment 4 which used training data only from sites within the same ecoregion (sites 2 and 3) to create an ecoregion model.
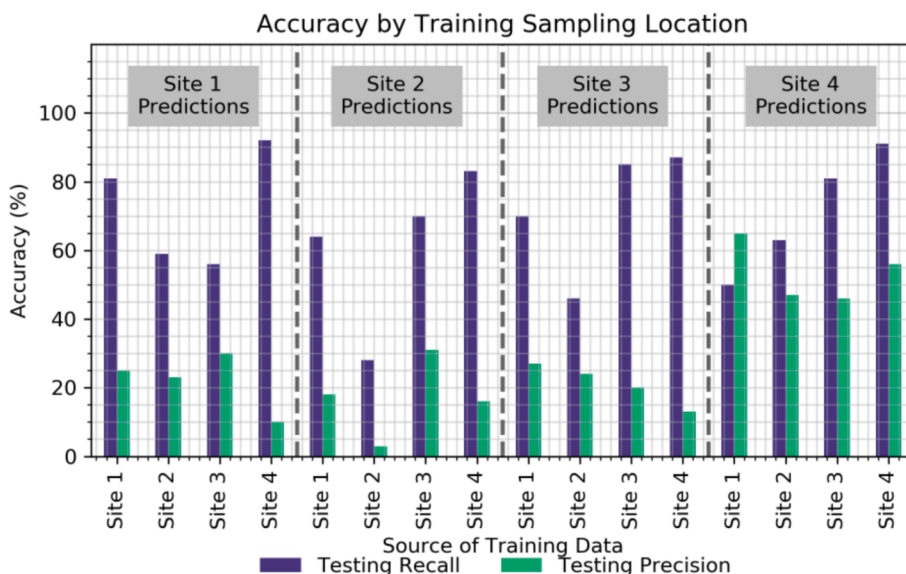

Fig. 5. Wetland mapping accuracy resulting from Experiment 2, where the best performing site-specific models were used to predict wetlands in other sites.

and 22%, respectively) compared to the general model, however this was not an improvement from the Site 3-specific model (Fig. 6). This suggests that an ecoregion-specific classification model may be useful, but not more so than a site-specific model given the data available here.

4. Discussion

4.1. Potential for site-specific models

We found that site-specific models improved as more training data was sampled from the area to be mapped, with the best models created from the maximum training datasets studied: 70% of the validation area. However, performance did not improve consistently for sites at the intermediate training data thresholds. This outcome exemplifies that model improvement is an issue of not only increasing the quantity of training data, but also the quality. The performance inconsistencies may be due to unequal wetland distributions in each training image. For example, the training images introduced for Site 1 when increasing the training data threshold from 9 to 28 images, may have provided very few wetland areas if the random selection included scenes with few or

only small wetlands. In addition, it is possible that the random nature of the training image set creation led to the introduction of some scenes with conflicting wetland/nonwetland signatures. As there is a benefit to identifying a training area threshold that begins to improve model performance across different sites, future work should include repeating this experiment with quality-controlled training data images and thresholds. Evaluating model performance across sites with training image thresholds at even increments of wetland and nonwetland area would result in more conclusive insights as to the changes in model performance as more training data becomes available. This being said, the overall improvements across the sites as training data increased to the maximum available set are likely due to the ability of the model to learn a wider range of wetland characteristics that exist in the additional landscape scenes.

Fig. 7 demonstrates the changes in wetland predictions as a result of increasing training data from nine training images (column A) to the maximum training images per site (column B). For sites 1, 3, and 4, increased training data reduced wetland overprediction surrounding the extents of ground truth wetlands, most notably for narrow wetland segments in sites 1 and 3. In addition, wetland predictions for these sites
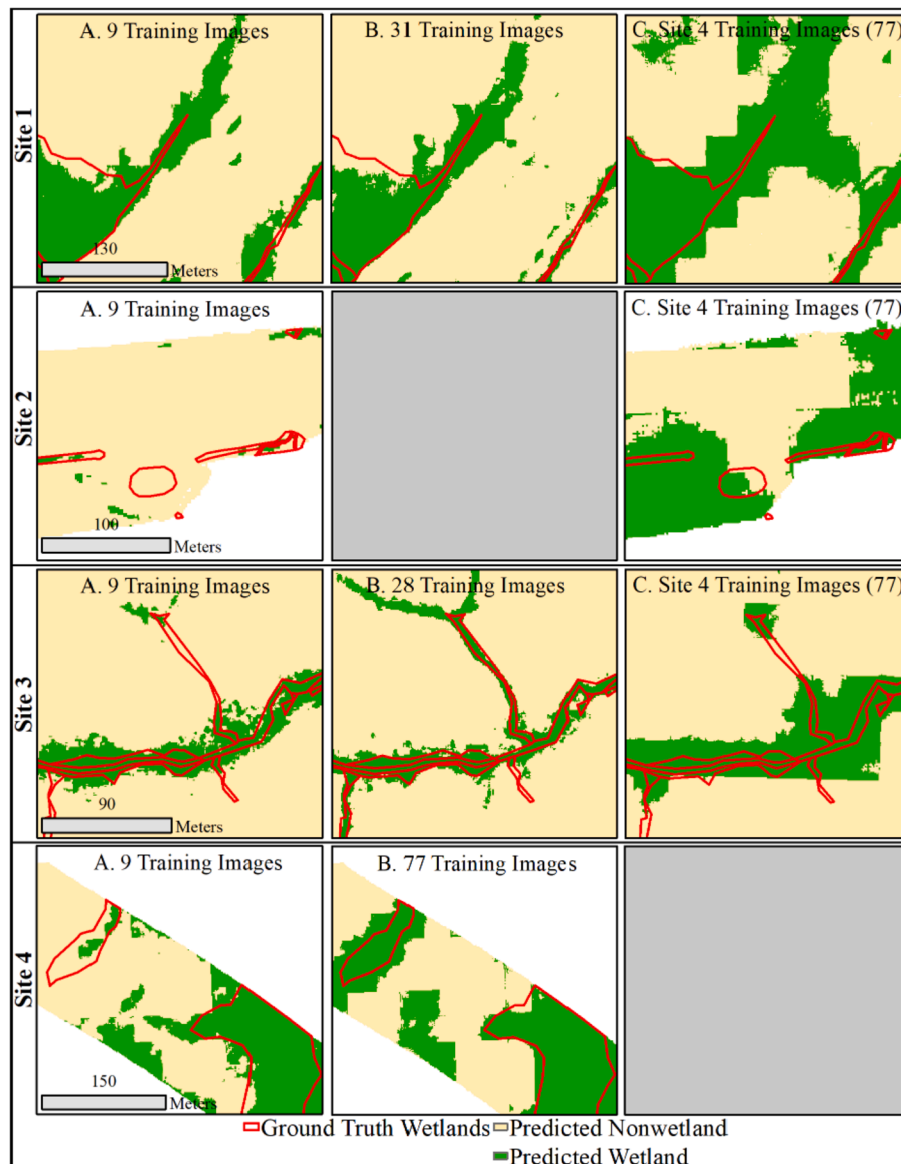

Fig. 7. Comparison of wetland predictions produced by site-specific models created from (column A) the smallest training dataset and (column B) the largest training dataset available for the site. Also shown are wetland predictions produced by models trained only with the largest training dataset for Site 4 (column C).

encompassed more of the true wetland area, most apparent for Site 4, where predictions densified for a relatively large wetland as a result of increasing the training data. Fig. 7 also exemplifies the poor performance of the Site 2 model. Although the Site 2 model predicts wetlands as small, linear features that are representative of the nature of ground truth wetlands in the area, the predictions are relatively sparse and incorrect. By visually examining the input features and testing data for Site 2, we found that validation wetlands existed underneath dense tree canopy along a road corridor. Topographic metrics in this area indicated values corresponding to wetness within the true wetland boundaries, however, the NDVI showed constant values for most of the forested area. The lack of distinction between values by the NDVI is likely due to the source imagery, the NAIP, which is collected during the growing season, with leaf-on conditions and is therefore affected by tree canopy. Moreover, the better performance for Site 4, even when using few training data, suggests that this landscape was particularly well-suited to the deep learning approach. This may be due to the large distribution of wetlands in Site 4, leading to a higher quantity of wetlands in the entire training data set as well as more significant presence of wetlands in each training image.

Fig. 7 also shows model predictions when using the Site 4-specific model. The Site 4 model produced predictions with the highest recall scores of all model trials for sites 1, 2, and 3. As indicated by the increases in recall, predictions resulting from the Site 4 more densely encompassed the ground truth wetlands (Fig. 7, column C), relative to results for the site-specific models (Fig. 7, columns A and B). Attributing to the lower precision scores also produced by the Site 4 model, wetland overprediction is apparent in the scenes for site 1, 2, and 3 (Fig. 7, column C). The wetland predictions for these sites are also made at a coarse resolution within image tile extents, evident by the rectangular edges of wetland predictions in sites 1 and 3 (Fig. 7, column C). In addition, a segment of a narrow wetland feature is omitted for Site 3 when applying the model trained for Site 4. Overall, these shortcomings demonstrate the potential for bias to a specific landscape and wetland type in site-specific models, which may lead to decreased accuracies when applied to different landscapes. This may be overcome by changing the classification strategy away from a simple wetland/non-wetland classification to one that classifies different wetland types, although this strategy was not explored through this research. The increase in recall scores when using the Site 4 model, and the
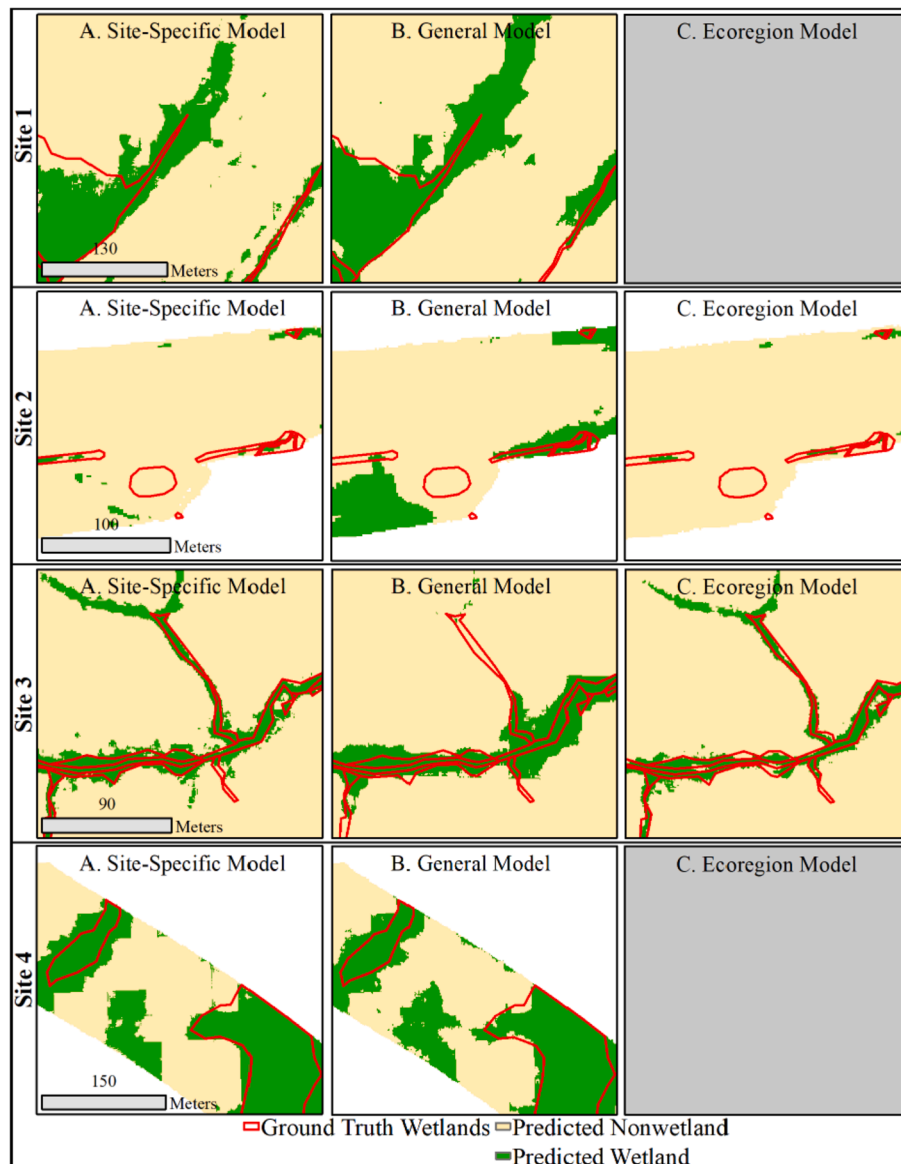

Fig. 8. Comparison of wetland predictions resulting by (column A) the best performing site-specific models (i.e., those trained on 70% of the validation area), (column B) the general model, and (column C) the ecoregion model.

concentration of wetland overprediction occurring in the adjacent and surrounding areas of the ground truth wetlands, suggests the noted shortcomings may also be addressed by using a more balanced sampling of different wetland types.

4.2. Potential for combined-site models

Compared to the site-specific models, the general model mostly resulted in more wetland overprediction, but in some cases increased coverage of ground truth wetlands (Fig. 8, column B). This trend is likely due to the bias of the general model to favor wetland types present in the Site 4 landscape, as more than half of all the training images used were from Site 4. While the general model results do not present an improvement from the site-specific models, there are improvements compared to wetland predictions resulting from a model trained only on Site 4 (see Fig. 7, column C). By supplementing the Site 4 training data with wetland information from other landscapes, we see finer, more precise wetland prediction boundaries (Fig. 8, Site 1 B and Site 3 B). For Site 2, the general model produced a greater overall amount of wetland predictions compared to the site-specific model, but predictions were inaccurate (Fig. 8, column A vs. column B). However, the quantity of erroneous wetland predictions for Site 2 was greater when using the Site 4 model versus the general model. It was expected that predictions for Site 4 would be mostly unchanged between the site-specific model and the general model, due to the significant presence of Site 4 training data. However, the weak training data influence from other sites did slightly improve precision for Site 4, demonstrated by finer-scale edges of wetland predictions (Fig. 8 Site 4 A vs. Site 4 B).

The ecoregion model explored the potential for creating combined-site models that are specific to certain landscape characteristics by including training data only from within the same ecoregion (i.e., sites 2 and 3). Fewer wetland predictions were made overall for Site 2 using the ecoregion model (Fig. 8, column C), which considerably reduced recall compared to the general model, but also resulted in sparser correct wetland predictions than the Site 2-specific model. For Site 3, the ecoregion model improved both precision and recall compared to the general model, but results were still less accurate than the site-specific model. Compared to general model predictions, the ecoregion model regained correct wetland predictions for narrow, riparian wetland features for Site 3 (Fig. 8, column C). The ecoregion model also reduced wetland overprediction compared to the general and site-specific models in the scenes shown in Fig. 8, representative of the higher precision produced by the ecoregion model (22% vs. 20% by the site-specific model and 15% by the general model). However, wetland predictions resulting from the ecoregion model encompassed less ground truth wetland area overall relative to the Site 3-specific model.

Although neither approach for creating a combined-site model was able to outperform site-specific models, results show potential to refine and improve these methods. We found that the relatively poor performances of the general and ecoregion models were not likely caused by the unequal sampling of training data from the different geographic study areas. To investigate this potential source of error, the general model and the ecoregion model were recreated by limiting training data from sites to just nine images each, balancing the representation from each site. For all sites, the general model built with equal, but limited training data performed worse than the proposed general model. For Site 3, the ecoregion model built with limited training data performed considerably worse, where recall decreased from 77% to 30% and precision improved slightly from 15% to 17%. For Site 2, however, the limited ecoregion model improved results slightly (recall increasing from 21 to 27% and precision remaining at 2%), but still not to an acceptable level of accuracy. Thus, improving the combined-site model approach may not just be a matter of equally sampling different landscapes, but also balancing an adequate amount of training data from different landscapes. Lastly, the lack of consistent improvement to Site 2 and Site 3 predictions when applying the ecoregion model suggests it

would be beneficial to consider additional landscape similarities when building combined-site models. Landscape characteristics to consider may be those that affect the distributions of topographic inputs, such as influence of built environment drainage and land cover.

4.3. Utility of the proposed input data configuration

This study explored an input data configuration unique to most deep learning applications where topographic derivatives of the input "image" (i.e., LiDAR DEM) are predetermined and specific to the target object (i.e., wetlands). The hypothesis was that predetermined elevation derivatives (TWI, DTW, and curvature) would improve wetland classification training by including hydrologic information, compared to training directly from the elevation data. To evaluate the efficacy of this method, we compared the accuracy achieved using our novel input data configuration versus two-band images composed of the LiDAR DEM and the NDVI, which is more representative of the common input data approach taken (e.g., Audebert et al., 2017, 2018; Latifovic et al., 2018; Liu et al., 2018; Silburt et al., 2018; Xu et al., 2018). The LiDAR DEMs used to create the two-band images were smoothed and hydrologically corrected, as suggested by O'Neil et al. (2019), and 70% of the areas were used for training for both model sets.

For sites 1, 2, and 3, the proposed input data configuration outperformed the typical approach in terms of both recall and precision. Wetlands predicted from only the DEM and NDVI for Site 1 achieved lower recall (73% vs. 81%) and precision (21% vs. 25%) compared to the models using the derived topographic indices and the NDVI. This suggests that combining physical understanding of the system, in this case hydrological and ecological characteristics of wetlands, helps to guide the deep learning algorithm so that it is able to obtain increased predictive skill. For Site 2, predictions learned from the DEM and NDVI encompassed only 12% of the ground truth wetlands with near 0% precision, compared to 28% recall and 3% precision achieved by the proposed approach. Wetland predictions for Site 3 lost considerable accuracy with the typical input data approach, producing 24% recall and 9% precision, whereas our approach resulted in 85% recall and 20% precision. For Site 4, this comparison showed that the model that learned from the DEM and NDVI alone produced a higher recall (96% vs. 91%) and lower precision (49% vs. 56%). While this indicates that more ground truth wetlands were detected using the typical approach, it is slightly outweighed by the loss in wetland precision. Considering the consistent improvement to the other three sites, the lack of significant change in Site 4 when applying only the DEM and NDVI may suggest that the deep learning model relies more heavily on the vegetative characteristics provided by the NDVI than the geomorphologic and hydrologic information that the elevation data offers. This is likely due to the fact that Site 4 had the least topographic relief, being within the coastal plain. Results for Site 4 using a random forest classification (see O'Neil et al., 2019) also support this idea, showing that the topographic input variables were insufficient for describing wetland characteristics unless preprocessing methods were calibrated specifically to the area. Thus, it is logical that wetlands in Site 4 are better described by vegetative characteristics than topography, explaining the lack of change in predictions when replacing the topographic inputs with the DEM and leaving the NDVI input unchanged.

4.4. Comparison of deep learning to a random forest implementation

To examine the potential for deep learning to advance the more commonly used random forest approach for wetland classification (e.g., O'Neil et al., 2019), we compared the performance of the site-specific deep learning models to a random forest classification with the same set of input variables. The random forest implementation follows the approach of O'Neil et al. (2019), but with the addition of the NDVI to the original set of inputs: the TWI, curvature, and DTW. The training sampling used in the O'Neil et al. (2019) study was maintained, where

training data consists of randomly dispersed pixels that encompass only 15% of the validated wetland area and up to 8% of the validated non-wetland area. However, accuracy assessments for both the deep learning and random forest models were limited to the extents of the testing image tiles that correspond to the deep learning approach.

Compared to the Site 1 deep learning model, the random forest classification resulted in an improvement in recall from 81% to 91%, but a decrease in precision from 25% to 19%. For Site 2, Random Forest improved recall considerably, from 28% to 78%, and slightly improved precision from 3% to 5%. The Site 3 random forest model produced no change in recall (85%) and a slight decrease in precision (20% vs. 18%), compared to deep learning. Finally, the Site 4 random forest model considerably decreased recall from 91% to 70% and increased precision from 56% to 64%, relative to the deep learning model. With the exception of Site 2, these findings show that deep learning was able to perform similarly to random forests (e.g., Site 1 and Site 3), and arguably better in some cases (e.g., Site 4). The poor performance in Site 2 further supports that the deep learning model was not sufficiently able to learn characteristics of wetland features that were very small and sparse relative to the landscape scenes in each training image. Similarly, the Site 4 results again support the idea that deep learning is better suited to detecting wetlands where they are areal and large relative to the landscape scene. In addition, an evaluation of the entire testing areas corresponding to the random forest models shows that the inclusion of the NDVI as a wetland indicator improves on the O'Neil et al. (2019) approach. Compared to the random forest models using only the topographic inputs, the addition of the NDVI improved wetland recall and precision in Site 1 (81% vs. 88% and 19% vs. 24%), Site 2 (82% vs. 88% and 16% vs. 22%), Site 3 (83% vs. 86% and 22% vs. 25%), and Site 4 (58% vs. 68% and 47% vs. 54%).

Overall, it is important to note that the random forest models were able to achieve these accuracies by sampling much less training data than was required for deep learning models. However, this result also shows that deep learning models can approach the same accuracies using training data resources that are considerably smaller relative to most deep learning applications. In addition, the similar performance of deep learning to random forests in three of the study sites supports findings by other researchers that state deep learning can improve landscape segmentation accuracy over traditional machine learning, such as support vector machine, maximum likelihood classification, and random forests, given enough training data (e.g., Hu et al., 2018; Latifovic et al., 2018; Liu et al., 2018; Mahdianpari et al., 2018).

4.5. Limitations

Limitations of this approach could be addressed through additional research. For example, incorporating Class Activation Mapping (CAM) (Zhou et al., 2016), which highlights scene elements that are most influential during classifications, would offer further insight into model learning. By utilizing CAM, model refinements could be made by quantifying the impact of the input data and identifying sources of error. Considering additional remote sensing data may also improve model performance. These may include LiDAR point clouds, which researchers have incorporated into 3-dimensional CNNs for wetland identification (e.g., Xu et al., 2018). Also, incorporating radar data may reduce errors where the NDVI is affected by tree canopy, as it is able to penetrate this layer and provide vegetation density and inundation information for wetland mapping (Allen et al., 2013; Behnamian et al., 2017; Corcoran et al., 2013; Kloiber et al., 2015; Millard and Richardson, 2013). Also on this point, the contribution of each input data source throughout the DeepNets workflow can be handled in a more sophisticated way. This was demonstrated by Audebert et al. (2018) who proposed novel data fusing methods for elevation data and the NDVI within the DeepNets workflow to improve land cover classifications.

Additional training information that consists of accurately delineated wetlands from across different ecoregions should improve the

deep learning classification results. Also, additional training data would make it possible to train models for specific wetland types rather than a simple, binary wetland/nonwetland classification. These training data are likely available from state and federal agencies given the need for wetland assessments under the Clean Water Act, but are not collected into a single, standardized repository. Future work could focus on building such a training and testing repository for wetland classification. Furthermore, to more efficiently make use of any amount of reliable training information available, applying more sophisticated data augmentation techniques may improve wetland predictions, as demonstrated by Stivaktakis et al. (2019).

Refinements to the current approach should also include more robust accuracy assessments. The current accuracy metrics are transparent and represent the two factors that are needed for reliable implementation: coverage of ground truth wetlands and limited overprediction. However, a single accuracy metric that encompasses both of these factors while also acknowledging the significantly higher importance of wetland recall would improve the interpretation of model results. Model evaluation improvements should also take into account the diffuse boundaries of wetlands which may fluctuate seasonally by penalizing overprediction less if it occurs adjacent to or surrounding defined ground truth wetland extents. Lastly, this study did not test the effect of tuning the DeepNets parameters. Among other parameter adjustments, future work should explore the benefit of adjusting window sizes based on target wetland size and the accuracy tradeoffs when training the model for more epochs.

5. Conclusions

We explore a wetland identification workflow that implements a basic semantic segmentation architecture and an input data configuration that consists of the NDVI and LiDAR DEM-derived indicators of wetland hydrology and geomorphology. The workflow was trained and evaluated using available data resources from four geographic regions of Virginia. From this work, we draw the following conclusions.

i. Site-specific deep learning models created from relatively small training datasets can achieve accurate results. For three of the four study sites, wetland recall ranged from 81 to 91% and precision ranged from 20 to 56%, when training models with 70% of site area and testing on the remaining 30% of the site area.

ii. Site-specific models were more successful for areas where wetlands are abundant and occupy a significant portion of training images. For a site with large, areal wetlands that were almost evenly balanced with nonwetland areas, high accuracy was achieved with 7.5 km^2 (70%) of training area (91% recall and 56% precision). Using a much smaller training area, 0.4 km^2 (10% of the study area), still resulted in a fairly accurate model (84% recall and 50% precision).

iii. In most cases, accuracy decreased when using models trained for another site. However, the site-specific model trained with the largest area studied (7.5 km^2) increased wetland recall in all other sites. Although model predictions were imprecise and showed a bias towards the types of wetlands for which it was trained (i.e., large, areal wetlands), the correct localization of wetland predictions suggests there is potential for this approach if models are trained with sufficient data and for areas with similar landscapes.

iv. Combined-site models can produce accurate wetland predictions, but training data contributions from the target landscapes should be balanced. The general model revealed the potential for bias towards landscape characteristics more heavily represented in the training data. However, the influence of less represented sites was still apparent, as wetland predictions were more inclusive of different wetland types compared to a model created without training data from these sites.

v. Shared ecoregion alone may not offer sufficient landscape similarities to improve the training sampling approach for combined-site models. The ecoregion model showed accuracy improvements from the general model for one site. However, wetland predictions for the other site were less accurate. Future work should explore the benefit of creating combined-site models from areas that share additional characteristics that would affect the distributions of the topographic derivatives, such as level of development, land cover, and topography.

vi. The proposed input data configuration improves wetland identification compared to a more typical approach of using the NDVI and the LiDAR DEM alone. By predetermining the derivatives of the DEM that are wetland indicators based on physical understanding of hydrology and wetland formation, rather than allowing the deep learning network to determine these through convolutions on raw data, wetland predictions were more accurate in three sites. This speaks to the benefit and power of combining physical understanding along with machine and deep learning algorithms for improved predictive skill. For the remaining site, accuracy was nearly unchanged between the two approaches. However, analyses show that this is likely due to the greater importance of the NDVI for identifying wetlands in the topographically mild landscape.

vii. Compared to a random forest approach, the best performing models produced comparable accuracy, using more training data than required for random forest, but still significantly less than what is typical in most deep learning applications.

Our results demonstrate the potential for deep learning to not only improve accuracy compared to traditional machine learning algorithms, but also provide flexible models that are accurate for a range of landscapes. Paramount to achieving this will be larger efforts within the research community to gather reliable training data and pretrained models stored as open source repositories, as has been done for established deep learning fields (e.g., Lecun, 1999; Lin et al., 2014). The wetland models created through this research may offer a starting point for creating a repository open to other researchers. By refining this implementation of the deep learning wetland workflow and further training the created models, there is potential for deep learning to support a range of wetland conservation efforts by producing accurate wetland inventories across many landscapes.

Software and data availability

Software created through this research along with documentation is available under an MIT license from https://github.com/uva-hydroinf ormatics/wetland_id. All input data required to run the model are publicly available through federal and state data providers. Wetland delineation datasets used for training and evaluation was made available to the researchers through a relationship with the Virginia Department of Transportation. To retrain the model for a new landscape, similar wetland delineation data for that area may be required.

Declaration of competing interest

The authors declare that they have no known competing financial interests or personal relationships that could have appeared to influence the work reported in this paper.

Acknowledgements

References

Ågren, A.M., Lidberg, W., Strömgren, M., Ogilvie, J., Arp, P.A., 2014. Evaluating digital terrain indices for soil wetness mapping-a Swedish case study. Hydrol. Earth Syst. Sci. 18 (9), 3623–3634. https://doi.org/10.5194/hess-18-3623-2014.

Ali, G., Birkel, C., Tetzlaff, D., Soulsby, C., Mcdonnell, J.J., Tarolli, P., 2014. A comparison of wetness indices for the prediction of observed connected saturated areas under contrasting conditions. Earth Surf. Process. Landforms 39 (3), 399–413. https://doi.org/10.1002/esp.3506.

Allen, T.R., Wang, Y., Gore, B., 2013. Coastal wetland mapping combining multi-date SAR and LiDAR. Geocarto Int. 28 (7), 616–631. https://doi.org/10.1080/10106049.2013.768297.

Audebert, N., Le Saux, B., Lefèvre, S., 2016. Semantic segmentation of earth observation data using multimodal and multi-scale deep networks. In: Asian Conference on Computer Vision. Springer, Cham, pp. 180–196.

Audebert, N., Le Saux, B., Lefèvre, S., 2017. Semantic segmentation of earth observation data using multimodal and multi-scale deep networks. In: Lai, S.-H., Lepetit, V., Nishino, K., Sato, Y. (Eds.), Computer Vision – ACCV 2016. Springer International Publishing, Cham, pp. 180–196. https://doi.org/10.1007/978-3-319-54181-5_12. Retrieved from.

Audebert, N., Le Saux, B., Lefèvre, S., 2018. Beyond RGB: very high resolution urban remote sensing with multimodal deep networks. ISPRS J. Photogrammetry Remote Sens. 140, 20–32. https://doi.org/10.1016/j.isprsjprs.2017.11.011.

Audebert, N., Le Saux, B., Lefèvre, S., 2019. Deep Learning for Earth Observation. Retrieved January 1, 2019, from. https://github.com/nshaud/DeepNetsForEO.

Badrinarayanan, V., Kendall, A., Cipolla, R., 2017. SegNet: a deep convolutional encoder-decoder architecture for image segmentation. IEEE Trans. Pattern Anal. Mach. Intell. 39 (12), 2481–2495. https://doi.org/10.1109/TPAMI.2016.2644615.

Baig, M.H.A., Zhang, L., Shuai, T., Tong, Q., 2014. Derivation of a tasselled cap transformation based on Landsat 8 at-satellite reflectance. Remote Sens. Lett. 5 (5), 423–431. https://doi.org/10.1080/2150704X.2014.915434.

Band, L.E., 1986. Topographic partition of watersheds with digital elevation models. Water Resour. Res. 22 (1), 15–24. https://doi.org/10.1029/WR022i001p00015.

Behnamian, A., Banks, S., White, L., Brisco, B., Millard, K., Pasher, J., et al., 2017. Semi-automated surfacewater detection with synthetic aperture radar data: a wetland case study. Rem. Sens. 9 (12), 1–21. https://doi.org/10.3390/rs9121209.

Beven, K.J., Kirkby, M.J., 1979. A physically based, variable contributing area model of basin hydrology/Un modèle à base physique de zone d'appel variable de l'hydrologie du bassin versant. Hydrol. Sci. Bull. 24 (1), 43–69. https://doi.org/10.1080/02626667909491834.

Boughorbel, S., Jarray, F., El-Anbari, M., 2017. Optimal classifier for imbalanced data using Matthews Correlation Coefficient metric. PloS One 12 (6), 1–17. https://doi.org/10.1371/journal.pone.0177678.

Branco, P., Torgo, L., Ribeiro, R.P., 2016. A survey of predictive modeling on imbalanced domains. ACM Comput. Surv. 49 (2), 1–50. https://doi.org/10.1145/2907070.

Byrt, T., Bishop, J., Carlin, J.B., 1993. Bias, prevalence and kappa. J. Clin. Epidemiol. 46 (5), 423–429. https://doi.org/10.1016/0895-4356(93)90018-V.

Carlson, T.N., Riziley, D.A., 1997. On the relation between NDVI, fractional vegetation cover, and leaf area index. Remote Sens. Environ. 62 (3), 241–252.

Chen, C., Liaw, A., Breiman, L., 2004. Using Random Forest to Learn Imbalanced Data (1999). University of California, Berkeley, pp. 1–12. ley.edu/sites/default/files/tech-reports/666.pdf.

Corcoran, J.M., Knight, J.F., Gallant, A.L., 2013. Influence of multi-source and multi-temporal remotely sensed and ancillary data on the accuracy of random forest classification of wetlands in northern Minnesota. Rem. Sens. 5 (7), 3212–3238. https://doi.org/10.3390/rs5073212.

Dahl, T.E., Johnson, C.E., Frayer, W.E., 1991. Wetlands, Status and Trends in the Conterminous United States Mid-1970's to Mid-1980's.

Davidson, N.C., 2014. How much wetland has the world lost? Long-term and recent trends in global wetland area. Mar. Freshw. Res. 65 (10), 934–941. https://doi.org/10.1071/MF14173.

Demir, I., Koperski, K., Lindenbaum, D., Pang, G., Huang, J., Basu, S., et al., 2018, June. Deepglobe 2018: a challenge to parse the earth through satellite images. In: 2018 IEEE/CVF Conference on Computer Vision and Pattern Recognition Workshops (CVPRW). IEEE, pp. 172–17209.

Deng, J., Smith, A.S., Davis, S., Weatherford, M., Paugh, L., Wang, S.-G., 2017. Identification of NC Wetland Types by LiDAR Data and Tree Based Machine Learning Methods (No. 17-01199).

Dronova, I., 2015. Object-based image analysis in wetland research: a review. Rem. Sens. 7 (5), 6380–6413. https://doi.org/10.3390/rs70506380.

Dronova, I., Gong, P., Wang, L., 2011. Object-based analysis and change detection of major wetland cover types and their classification uncertainty during the low water period at Poyang Lake, China. Remote Sens. Environ. 115 (12), 3220–3236. https://doi.org/10.1016/j.rse.2011.07.006.

Farm Service Agency, 2017. National geospatial data asset (NGDA) national agriculture imagery program (NAIP) imagery. Retrieved January 1, 2019, from. https://catalog.data.gov/dataset/national-geospatial-data-asset-ngda-naip-imagery.

Ghosh, A., Ehrlich, M., Shah, S., Davis, L.S., Chellappa, R., 2018. June). Stacked U-nets for ground material segmentation in remote sensing imagery. In: CVPR Workshops, pp. 257–261.

GRASS Development Team, 2017. Geographic Resources Analysis Support System (GRASS GIS) Software. Version 7.2. Retrieved from. http://grass.osgeo.org.

Grimaldi, S., Nardi, F., Benedetto, F. Di, Istanbulluoglu, E., Bras, R.L., 2007. A physically-based method for removing pits in digital elevation models. Adv. Water Resour. 30 (10), 2151–2158. https://doi.org/10.1016/j.advwatres.2006.11.016.

Guo, M., Li, J., Sheng, C., Xu, J., Wu, L., 2017. A review of wetland remote sensing. Sensors 17 (4), 1–36. https://doi.org/10.3390/s17040777.

Hart, P.E., Nilsson, N.J., Raphael, B., 1968. Formal basis for the heuristic determination eijj. Syst. Sci. Cybern. (2), 100–107.

He, K., Zhang, X., Ren, S., Sun, J., 2016. Deep residual learning for image recognition. In: IEEE Conference on Computer Vision and Pattern Recognition, pp. 770–778. Retrieved from. http://arxiv.org/abs/1512.03385.

Hinton, G.E., Osindero, S., Teh, Y.-W., 2006. A fast learning algorithm for deep belief nets. Neural Comput. 18 (7), 1527–1554. https://doi.org/10.1162/neco.2006.18.7.1527.

Hogg, A.R., Todd, K.W., 2007. Automated discrimination of upland and wetland using terrain derivatives. Can. J. Rem. Sens. 33 (July), S68–S83. https://doi.org/10.5589/m07-049.

Holmgren, P., 1994. Multiple flow direction algorithms for runoff modelling in grid based elevation models: an empirical evaluation. Hydrol. Process. 8 (4), 327–334. https://doi.org/10.1002/hyp.3360080405.

Hu, Y., Zhang, Q., Zhang, Y., Yan, H., 2018. A deep convolution neural network method for land cover mapping: a case study of qinhuangdao, China. Rem. Sens. 10 (12), 2053. https://doi.org/10.3390/rs10122053.

Jenson, S.K., Domingue, J.O., 1988. Extracting topographic structure from digital elevation data for geographic information system analysis. Photogramm. Eng. Rem. Sens. 54 (11), 1593–1600, 0099-1112/88/5411-1593$02.25/0.

Jyotsna, R., Haff, P.K., 1997. Microtopography as an indicator of modern hillslope diffusivity in arid terrain. Geology 25 (8), 695–698. https://doi.org/10.1130/0091-7613(1997)025%3C0695:MAAIOM%3E2.3.CO. Retrieved from.

Kemker, R., Salvaggio, C., Kanan, C., 2018a. Algorithms for semantic segmentation of multispectral remote sensing imagery using deep learning. ISPRS J. Photogrammetry Remote Sens. 145 (April), 60–77. https://doi.org/10.1016/j.isprsjprs.2018.04.014.

Kemker, R., Gewali, U.B., Kanan, C., 2018b. EarthMapper: a tool box for the semantic segmentation of remote sensing imagery. Retrieved from. http://arxiv.org/abs/1804.00292, 1-5.

Kim, M., Warner, T.A., Madden, M., Atkinson, D.S., 2011. Multi-scale GEOBIA with very high spatial resolution digital aerial imagery: scale, texture and image objects. Int. J. Rem. Sens. 32 (10), 2825–2850.

Klemas, V., 2011. Remote sensing of wetlands: case studies comparing practical techniques. J. Coast Res. 27 (3), 418–427. https://doi.org/10.2112/JCOASTRES-D-10-00174.1.

Kloiber, S.M., Macleod, R.D., Smith, A.J., Knight, J.F., Huberty, B.J., 2015. A semi-automated, multi-source data fusion update of a wetland inventory for east-central Minnesota, USA. Wetlands 35 (2), 335–348. https://doi.org/10.1007/s13157-014-0621-3.

Krizhevsky, A., Sutskever, I., Hinton, G.E., 2017. ImageNet classification with deep convolutional neural networks. Commun. ACM 60 (6), 84–90. https://doi.org/10.1145/3065386.

Lang, M., McCarty, G., 2014. Light Detection and Ranging (LiDAR) for Improved Mapping of Wetland Resources and Assessment of Wetland Conservation Projects, (September), p. 7. Retrieved from. http://www.nrcs.usda.gov/Internet/FSE_DOCUMENTS/stelprdb1260970.pdf.

Lang, M., McCarty, G., Oesterling, R., Yeo, I.Y., 2013. Topographic metrics for improved mapping of forested wetlands. Wetlands 33 (1), 141–155. https://doi.org/10.1007/s13157-012-0359-8.

Latifovic, R., Pouliot, D., Campbell, J., 2018. Assessment of convolution neural networks for surficial geology mapping in the south rae geological region, northwest territories, Canada. Rem. Sens. 10 (2), 307. https://doi.org/10.3390/rs10020307.

Lecun, Y., 1999. THE MNIST DATABASE of Handwritten Digits. Retrieved from. https://ci.nii.ac.jp/naid/10027939599/en/.

LeCun, Y., Bottou, L., Bengio, Y., Haffner, P., others, 1998. Gradient-based learning applied to document recognition. Proc. IEEE 86 (11), 2278–2324.

Lee, C. suk, Sohn, E., Park, J.D., Jang, J.-D., 2019. Estimation of soil moisture using deep learning based on satellite data: a case study of South Korea. GIScience Remote Sens. 56 (1), 43–67. https://doi.org/10.1080/15481603.2018.1489943.

Lin, T.-Y., Maire, M., Belongie, S., Hays, J., Perona, P., Ramanan, D., et al., 2014. Microsoft coco: common objects in context. In: European Conference on Computer Vision, pp. 740–755.

Lindsay, J.B., 2016. Efficient hybrid breaching-filling sink removal methods for flow path enforcement in digital elevation models. Hydrol. Process. 30 (6), 846–857. https://doi.org/10.1002/hyp.10648.

Lindsay, J.B., Creed, I.F., 2005. Removal of artifact depressions from digital elevation models: towards a minimum impact approach. Hydrol. Process. 19 (16), 3113–3126. https://doi.org/10.1002/hyp.5835.

Liu, T., Abd-Elrahman, A., Morton, J., Wilhelm, V.L., 2018. Comparing fully convolutional networks, random forest, support vector machine, and patch-based deep convolutional neural networks for object-based wetland mapping using images from small unmanned aircraft system. GIScience Remote Sens. 55 (2), 243–264. https://doi.org/10.1080/15481603.2018.1426091.

Long, J., Shelhamer, E., Darrell, T., 2015. Fully convolutional networks for semantic segmentation. In: Proceedings of the IEEE Conference on Computer Vision and Pattern Recognition, pp. 3431–3440.

Ma, L., Li, M., Ma, X., Cheng, L., Du, P., Liu, Y., 2017. A review of supervised object-based land-cover image classification. ISPRS J. Photogrammetry Remote Sens. 130, 277–293. https://doi.org/10.1016/j.isprsjprs.2017.06.001.

Mahdianpari, M., Salehi, B., Rezaee, M., Mohammadimanesh, F., Zhang, Y., 2018. Very deep convolutional neural networks for complex land cover mapping using multispectral remote sensing imagery. Rem. Sens. 10 (7), 1119. https://doi.org/10.3390/rs10071119.

Marmanis, D., Schindler, K., Wegner, J.D., Galliani, S., Datcu, M., Stilla, U., 2018. Classification with an edge: improving semantic image segmentation with boundary detection. ISPRS J. Photogrammetry Remote Sens. 135, 158–172. https://doi.org/10.1016/j.isprsjprs.2017.11.009.

Metz, M., Mitasova, H., Harmon, R.S., 2011. Efficient extraction of drainage networks from massive, radar-based elevation models with least cost path search. Hydrol. Earth Syst. Sci. 15 (2), 667–678. https://doi.org/10.5194/hess-15-667-2011.

Millard, K., Richardson, M., 2013. Wetland mapping with LiDAR derivatives, SAR polarimetric decompositions, and LiDAR-SAR fusion using a random forest classifier. Can. J. Rem. Sens. 39 (4), 290–307. https://doi.org/10.5589/m13-038.

Millard, K., Richardson, M., 2015. On the importance of training data sample selection in Random Forest image classification: a case study in peatland ecosystem mapping. Rem. Sens. 7 (7), 8489–8515. https://doi.org/10.3390/rs70708489.

Moore, I.D., Grayson, R.B., Ladson, A.R., 1991. Digital terrain modelling: a review of hydrological, geomorphological, and biological applications. Hydrol. Process. 5 (1), 3–30. https://doi.org/10.1002/hyp.3360050103.

Mui, A., He, Y., Weng, Q., 2015. An object-based approach to delineate wetlands across landscapes of varied disturbance with high spatial resolution satellite imagery. ISPRS J. Photogrammetry Remote Sens. 109, 30–46. https://doi.org/10.1016/j.isprsjprs.2015.08.005.

Murphy, P.N.C., Ogilvie, J., Connor, K., Arp, P.A., 2007. Mapping wetlands: a comparison of two different approaches for New Brunswick, Canada. Wetlands 27 (4), 846–854. https://doi.org/10.1672/0277-5212(2007)27[846:MWACOT]2.0.CO;2.

Murphy, P.N.C., Ogilvie, J., Arp, P., 2009. Topographic modelling of soil moisture conditions: a comparison and verification of two models. Eur. J. Soil Sci. 60 (1), 94–109. https://doi.org/10.1111/j.1365-2389.2008.01094.x.

Murphy, P.N.C., Ogilvie, J., Meng, F.R., White, B., Bhatti, J.S., Arp, P.A., 2011. Modelling and mapping topographic variations in forest soils at high resolution: a case study. Ecol. Model. 222 (14), 2314–2332. https://doi.org/10.1016/j.ecolmodel.2011.01.003.

Oltean, G.S., Comeau, P.G., White, B., 2016. Linking the depth-to-water topographic index to soil moisture on boreal forest sites in Alberta. For. Sci. 62 (2), 154–165. https://doi.org/10.5849/forsci.15-054.

Ozesmi, S.L., Bauer, M.E., 2002. Satellite remote sensing of wetlands. Wetl. Ecol. Manag. 10 (5), 381–402.

O'Callaghan, J.F., Mark, D.M., 1984. The extraction of drainage networks from digital elevation data. Comput. Vis. Graph Image Process 28 (3), 323–344. https://doi.org/10.1016/S0734-189X(84)80011-0.

O'Neil, G.L., Goodall, J.L., Watson, L.T., 2018. Evaluating the potential for site-specific modification of LiDAR DEM derivatives to improve environmental planning-scale wetland identification using Random Forest classification. J. Hydrol. 559, 192–208. https://doi.org/10.1016/j.jhydrol.2018.02.009.

O'Neil, G.L., Saby, L., Band, L.E., Goodall, J.L., 2019. Effects of LiDAR DEM smoothing and conditioning techniques on a topography-based wetland model. Water Resour. Res. https://doi.org/10.1029/2019WR024784, 2019WR024784.

Page, R.W., Wilcher, L.S., 1990. Memorandum of Agreement between the Environmental Protection Agency and the Department of the Army Concerning the Determination of Mitigation under the Clean Water Act, Section 404 (B)(1) Guidelines (Washington, DC, USA).

Pan, B., Hsu, K., AghaKouchak, A., Sorooshian, S., 2019. Improving precipitation estimation using convolutional neural network. Water Resour. Res. 55 (3), 2301–2321. https://doi.org/10.1029/2018WR024090.

Passalacqua, P., Do Trung, T., Foufoula-Georgiou, E., Sapiro, G., Dietrich, W.E., 2010a. A geometric framework for channel network extraction from lidar: nonlinear diffusion and geodesic paths. J. Geophys. Res. 115 (F1), F01002. https://doi.org/10.1029/2009JF001254.

Passalacqua, P., Tarolli, P., Foufoula-Georgiou, E., 2010b. Testing space-scale methodologies for automatic geomorphic feature extraction from lidar in a complex mountainous landscape. Water Resour. Res. 46 (11), 1–17. https://doi.org/10.1029/2009WR008812.

Passalacqua, P., Belmont, P., Foufoula-Georgiou, E., 2012. Automatic geomorphic feature extraction from lidar in flat and engineered landscapes. Water Resour. Res. 48 (3), 1–18. https://doi.org/10.1029/2011WR010958.

Paszke, A., Gross, S., Chintala, S., Chanan, G., Yang, E., DeVito, Z., et al., 2017. Automatic differentiation in PyTorch. In: NIPS Autodiff Workshop.

Perona, P., Malik, J., 1990. Scale-space and edge detection using anisotropic diffusion. IEEE Trans. Pattern Anal. Mach. Intell. 12 (7), 629–639. https://doi.org/10.1109/34.56205.

PyGeoNet, 2019. Retrieved August 1, 2018, from. https://github.com/passaH2O/GeoNet.

Rampi, L.P., Knight, J.F., Pelletier, K.C., 2014. Wetland mapping in the upper midwest United States. Photogramm. Eng. Rem. Sens. 80 (5), 439–448. https://doi.org/10.14358/pers.80.5.439.

Rezaee, M., Mahdianpari, M., Zhang, Y., Salehi, B., 2018. Deep convolutional neural network for complex wetland classification using optical remote sensing imagery. IEEE J. Selected Top. Appl. Earth Observ. Remote Sens. 11 (9), 3030–3039. https://doi.org/10.1109/JSTARS.2018.2846178.

Sangireddy, H., Stark, C.P., Kladzyk, A., Passalacqua, P., 2016. GeoNet: an open source software for the automatic and objective extraction of channel heads, channel network, and channel morphology from high resolution topography data. Environ. Model. Software 83, 58–73. https://doi.org/10.1016/j.envsoft.2016.04.026.

Scikit-learn Developers, 2017. Model Evaluation: Quantifying the Quality of Predictions. Retrieved from. http://scikit-learn.org/stable/modules/model_evaluation.html.

Scott, G.J., England, M.R., Starms, W.A., Marcum, R.A., Davis, C.H., 2017. Training deep convolutional neural networks for land-cover classification of high-resolution imagery. Geosci. Rem. Sens. Lett. IEEE 14 (4), 549–553. https://doi.org/10.1109/LGRS.2017.2657778.

Serre, T., Kreiman, G., Kouh, M., Cadieu, C., Knoblich, U., Poggio, T., 2007. A quantitative theory of immediate visual recognition. Prog. Brain Res. 165, 33–56. https://doi.org/10.1016/S0079-6123(06)65004-8.

Shen, C., 2018. A transdisciplinary review of deep learning research and its relevance for water resources scientists. Water Resour. Res. 54 (11), 8558–8593. https://doi.org/10.1029/2018WR022643.

Silburt, A., Ali-dib, M., Zhu, C., Jackson, A., 2018. Lunar Crater Identification via Deep Learning.

Simonyan, K., Zisserman, A., 2014. Very Deep Convolutional Networks for Large-Scale Image Recognition. ArXiv Preprint ArXiv:1409.1556.

Snyder, G.I., Lang, M., 2012. Significance of a 3D elevation program to wetland mapping. Natl. Wetl. Newsl. 34 (5), 11–15. Retrieved from. http://pubs.er.usgs.gov/publication/70193349.

Stivaktakis, R., Tsagkatakis, G., Tsakalides, P., 2019. Deep learning for multilabel land cover scene categorization using data augmentation. Geosci. Rem. Sens. Lett. IEEE 16 (7), 1–5. https://doi.org/10.1109/lgrs.2019.2893306.

Sun, Y., Kamel, M.S., Wong, A.K.C., Wang, Y., 2007. Cost-sensitive boosting for classification of imbalanced data. Pattern Recogn. 40 (12), 3358–3378. https://doi.org/10.1016/j.patcog.2007.04.009.

Tarboton, D.G., 1991. On the extraction of channel networks from digital elevation data. Hydrol. Process. 5 (1), 81–100. https://doi.org/10.1002/hyp.3360050107.

Tian, S., Zhang, X., Tian, J., Sun, Q., 2016. Random forest classification of wetland landcovers from multi-sensor data in the arid region of Xinjiang, China. Rem. Sens. 8 (11), 954. https://doi.org/10.3390/rs8110954.

US Corps of Engineers, 1987. Corps of Engineers Wetlands Delineation Manual and Regional Supplements. US Army Engineer Waterways Experiment Station Vicksburg, Mississippi. Retrieved from. http://www.epa.gov/cwa-404/section-404-clean-water-act-how-wetlands-are-defined-and-identified.

USGS, 2019. USGS National Hydrography Dataset. Retrieved August 1, 2017, from. https://www.usgs.gov/core-science-systems/ngp/national-hydrography/national-hydrography-dataset.

(VITA), V. I. T. A., 2016. Virginia Base Map Data Downloads from. http://vgin.maps.arcgis.com. (Accessed 1 August 2016).

Volpi, M., Tuia, D., 2016. Dense semantic labeling of subdecimeter resolution images with convolutional neural networks. IEEE Trans. Geosci. Rem. Sens. https://doi.org/10.1109/TGRS.2016.2616585.

White, B., Ogilvie, J., Campbell, D.M.H., Hiltz, D., Gauthier, B., Chisholm, H.K., et al., 2012. Using the cartographic depth-to-water index to locate small streams and associated wet areas across landscapes. Can. Water Resour. J. 37 (4), 333–347. https://doi.org/10.4296/cwrj2011-909.

Woodrow, K., Lindsay, J.B., Berg, A.A., 2016. Evaluating DEM conditioning techniques, elevation source data, and grid resolution for field-scale hydrological parameter extraction. J. Hydrol. 540, 1022–1029. https://doi.org/10.1016/j.jhydrol.2016.07.018.

Xu, Z., Guan, K., Casler, N., Peng, B., Wang, S., 2018. A 3D convolutional neural network method for land cover classification using LiDAR and multi-temporal Landsat imagery. ISPRS J. Photogrammetry Remote Sens. 144 (August), 423–434. https://doi.org/10.1016/j.isprsjprs.2018.08.005.

Zhang, L., Zhang, L., Du, B., 2016. Deep learning for remote sensing data: a technical tutorial on the state of the art. IEEE Geosci. Remote Sens. Mag. 4 (2), 22–40. https://doi.org/10.1109/MGRS.2016.2540798.

Zhou, B., Khosla, A., Lapedriza, A., Oliva, A., Torralba, A., 2016. Learning Deep Features for Discriminative Localization. Retrieved from. http://arxiv.org/abs/1512.04150.

Zhu, J., Pierskalla, W.P., 2016. Applying a weighted random forests method to extract karst sinkholes from LiDAR data. J. Hydrol. 533, 343–352. https://doi.org/10.1016/j.jhydrol.2015.12.012.